25. Y. S. Park, H. L. Wang, *Nat. Phys.* **5**, 489 (2009).
26. A. H. Safavi-Naeini, O. Painter, *N. J. Phys.* **13**, 013017 (2011).
27. D. E. Chang, A. H. Safavi-Naeini, M. Hafezi, O. Painter, *N. J. Phys.* **13**, 023003 (2011).
28. J. D. Thompson *et al.*, *Nature* **452**, 72 (2008).
29. G. Anetsberger *et al.*, *Nat. Phys.* **5**, 909 (2009).
30. P. Rabl *et al.*, *Nat. Phys.* **6**, 602 (2010).
31. P. Treutlein, D. Hunger, S. Camerer, T. W. Hänsch, J. Reichel, *Phys. Rev. Lett.* **99**, 140403 (2007).
32. S. Kolkowitz *et al.*, *Science* **335**, 1603 (2012); 10.1126/science.1216821.
33. J. T. Hill, A. H. Safavi-Naeini, J. Chan, O. Painter, *Nat. Comm.* **3**, 1196 (2012).

Acknowledgment: This work is supported by the Defense Advanced Research Projects Agency ORCHID (Optical Radiation Cooling and Heating in Integrated Devices) program through a grant from Air Force Office for Scientific Research and by NSF.

Supplementary Materials
www.sciencemag.org/cgi/content/full/science.1228370/DC1
Materials and Methods
Supplementary Text
Figs. S1 to S9
References

3 August 2012; accepted 5 November 2012
Published online 15 November 2012;
10.1126/science.1228370

Porphyry-Copper Ore Shells Form at Stable Pressure-Temperature Fronts Within Dynamic Fluid Plumes

P. Weis,[1]* T. Driesner,[1] C. A. Heinrich[1,2]

Porphyry-type ore deposits are major resources of copper and gold, precipitated from fluids expelled by crustal magma chambers. The metals are typically concentrated in confined ore shells within vertically extensive vein networks, formed through hydraulic fracturing of rock by ascending fluids. Numerical modeling shows that dynamic permeability responses to magmatic fluid expulsion can stabilize a front of metal precipitation at the boundary between lithostatically pressured up-flow of hot magmatic fluids and hydrostatically pressured convection of cooler meteoric fluids. The balance between focused heat advection and lateral cooling controls the most important economic characteristics, including size, shape, and ore grade. This self-sustaining process may extend to epithermal gold deposits, venting at active volcanoes, and regions with the potential for geothermal energy production.

Porphyry-type ore deposits are among the world's premier metal resources, supplying most of the copper, molybdenum, and a substantial part of gold production (*1*). They form in response to focused expulsion of metal-bearing saline fluids from large chambers of cooling hydrous magma (*2*). A restricted zone of ore-mineral precipitation within a more extensive plume of fluid up-flow is thought to be the key to economic metal accumulation (*3*). The ore typically forms well-defined bodies of bell-like or cylindrical shape, centered on dike- or stocklike porphyry intrusions at some distance above cupolas in the roof of magma chambers (Fig. 1) (*1*, *4*–*7*). Geological observations and fluid inclusion data indicate physical and chemical processes of a dynamic flow system that resemble volcanic systems at the verge of eruption (*8*, *9*).

The top of the ore shell is commonly abrupt and coincides with the top of a dense vein network (*1*), indicating that fluid pressures were sufficient to induce hydraulic fracturing. The core within and below the ore shell is veined but barren and commonly hosts fluid inclusions with intermediate density, interpreted to represent a hot (>600°C), near-lithostatically pressured single-phase fluid that ascended from the subjacent magma chamber (*7*). On ascent, this primary magmatic fluid separates into a low-salinity vapor and a high-salinity liquid phase, recorded by ubiquitous vapor and brine inclusions in all porphyry deposits (*1*, *7*). The physical mechanism creating a zone of localized chemical precipitation during the lifetime of the system is key to metal enrichment to economic grades but remains elusive.

Here, we present numerical simulations of the physical hydrology of porphyry systems that link the expulsion of saline magmatic fluids with the transient evolution of rock permeability and the dynamics of two-phase fluid flow (*10*). The geometric configuration of our model is a two-dimensional (2D) representation of a 10- by 3-km magma chamber of elliptical shape with a cupola in the roof at 5 km depth (Fig. 2A). It has been constructed to resemble the dimensions of the Yerington porphyry system (Fig. 1B), which shows the most complete and best mapped exposure from a deep source pluton to the paleosurface. We compute the expulsion rates to be proportional to the rate of magma crystallization and release saline magmatic fluids through the cupola zone of a 3D magma chamber (*10*) (fig. S1).

Our model is based on published constitutive relationships and empirical parameterizations of the effects of brittle, ductile, and elastic rock mechanics on crustal permeability in a continuum porous-media approach (Fig. 2) (*10*). The model links a critically stressed crust with an average depth-dependent permeability profile (*11*, *12*). Superimposed on this background behavior, permeability closes at temperatures above the brittle-ductile transition (*13*, *14*) and opens at fluid pressures exceeding a criterion for rock failure (*15*), which varies from near-hydrostatic for brittle rock to near-lithostatic for ductile rock (Fig. 2). The model generates a dynamic hydrothermal system with varying domains of brittle and ductile rock behavior, solely from these initial conditions and geologically realistic descriptions of material properties.

The simulations demonstrate a self-sustaining mechanism that can stabilize a front of copper precipitation in porphyry deposits, which is con-

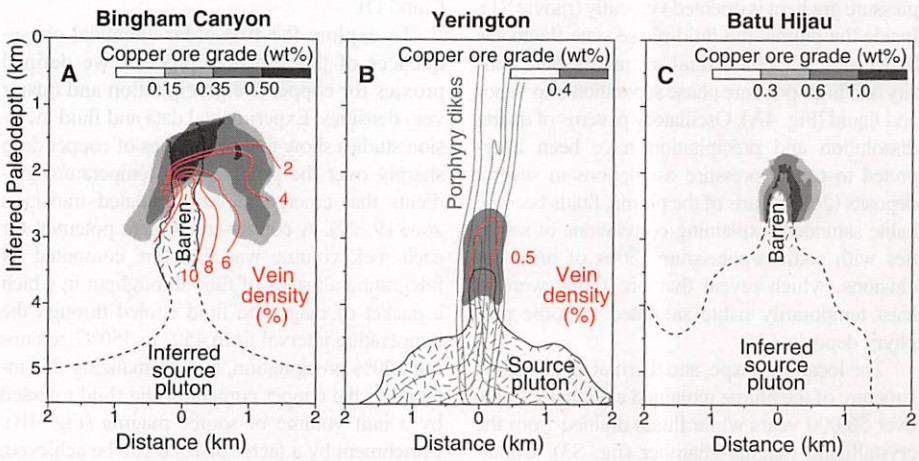

Fig. 1. Characteristic ore shells and vein densities of porphyry-style deposits. **(A)** Bingham Canyon, Utah, USA (*6*, *7*). **(B)** Yerington, Nevada, USA (*5*). **(C)** Batu Hijau, Indonesia (*4*). Figures are simplified from published field observations and reconstructed geology.

[1]Department of Earth Sciences, Eidgenössische Technische Hochschule (ETH) Zurich, 8092 Zürich, Switzerland. [2]Faculty of Mathematics and Natural Sciences, University of Zurich, 8006 Zürich, Switzerland.

*To whom correspondence should be addressed. E-mail: weis@erdw.ethz.ch

sistent with their characteristic zoning patterns. The interplay of permeability, heat advection, and nonlinear fluid properties establishes a vertically extensive up-flow zone of magmatic fluids (Fig. 3). It is characterized by a hot inner part with near-lithostatic pressures, which is overlain and surrounded by cooler parts with meteoric water convecting under hydrostatic conditions. A self-sealing rim of low permeability develops in response to the opposing permeability effects of the two fluid regimes. In the inner part, high temperatures above the brittle-ductile transition are maintained by the continuous supply of hot magmatic fluid, lowering permeability and keeping fluid pressures high. From outside, convection of meteoric fluids removes heat and shapes the sides of the plume. Their subvertical orientation is the result of an interplay of fluid and rock at temperatures between 350° and 400°C, at which the brittle-ductile transition starts (*16*) and strong gradients in fluid properties tend to maximize vertical, advective heat transport (*17*, *18*). Heat transfer from the inner part of the plume to the convecting meteoric fluids on the sides is mainly by conduction through the low-permeability transition zone. Toward the upper part of the plume, meteoric convection becomes more intense in response to the increase in permeability of the host rock along the depth-dependent background profile (Fig. 2D) and leads to formation of the rounded top of the high-pressure, high-temperature part of the plume (Fig. 3A).

During volatile expulsion, magmatic fluids move through the hot plume in rapid overpressure-permeability waves (Fig. 3). At the injection location above the cupola, permeability is insufficient to accommodate the supply of magmatic volatiles at pressures below the failure criterion, which leads to wavelike behavior when applying an incremental hydrofracturing model that relates permeability changes to the amount of overpressure (*10*, *19*). Even though our model does not explicitly include permeability anisotropy, a vertical movement of the overpressure-permeability waves develops naturally because the strongest (lithostatic) fluid pressure gradient is oriented vertically (movie S1). Inside the plume, the fluid-phase state fluctuates between single-phase fluid of intermediate density and high-pressure phase separation into vapor and liquid (Fig. 4A). Oscillatory patterns of quartz dissolution and precipitation have been interpreted to reflect pressure oscillations in several deposits (*20*). In parts of the plume, fluids become halite saturated, explaining correlations of salinities with sodium/potassium ratios of brine inclusions, which reveal that ore fluids were at least temporarily halite saturated in some porphyry deposits (*21*).

The location, shape, and thermal and pressure structure of the plume remained essentially stable over 50,000 years while fluids drained from the crystallizing magma chamber (fig. S3). Conditions in the upper parts closely resemble those inferred for porphyry copper ore deposition: When a magmatic fluid pulse crosses the transition zone between the magmatic and meteoric fluid regimes, pressure drops from above lithostatic to hydrostatic, and temperature decreases from above 500°C to below 350°C within about 200 m (Fig. 3, C and D).

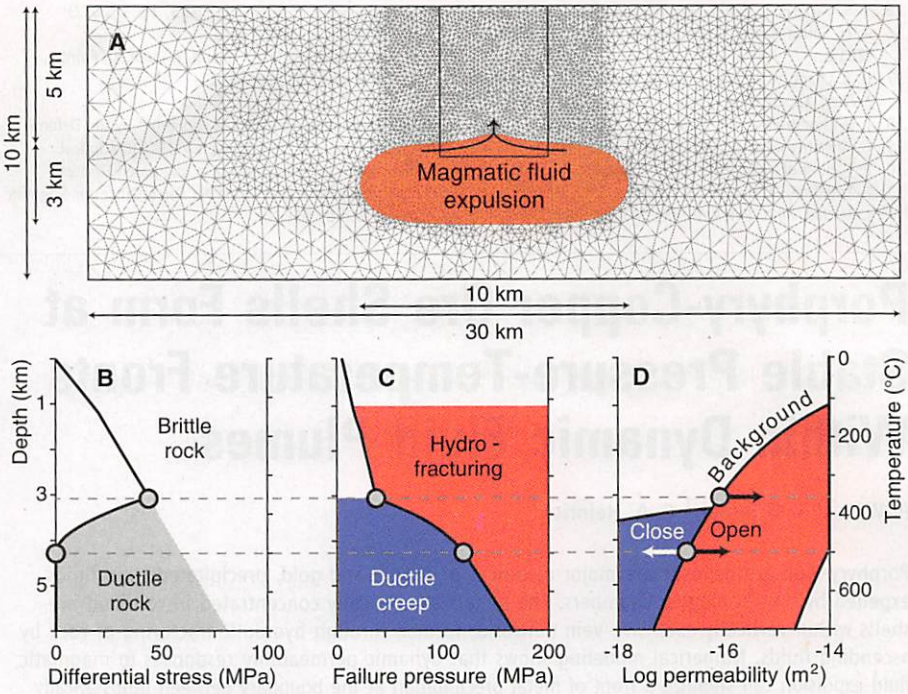

Fig. 2. Model configuration. **(A)** The mesh consists of ~9000 triangular elements with the finest resolution (50 m) above the magma chamber. The box in the center marks the location of the 4- by 5.5-km excerpt in Figs. 3A and 4. **(B)** The crust is assumed to be near-critically stressed (*12*); differential stress increases with depth (left axis). The stress field is not varied in our model but responds to thermal conditions so as to mimic the transition from brittle to ductile rock (*13*), exemplified with a schematic temperature gradient reaching magmatic temperatures (right axis). **(C)** Failure pressure defines a stress-state–dependent criterion for rock failure (*15*). Fluid pressures exceeding failure pressure will hydrofracture the rock (red). Ductile creep dominates at elevated temperatures and fluid pressures below this failure criterion (blue). **(D)** Background permeability follows a depth-dependent profile for average continental crust (*11*). Permeability opens incrementally during hydrofracturing (black arrow) and is reduced to the background value after overpressure release. At temperatures above the brittle–ductile transition, permeability closes, mimicking the loss of interconnected pore space due to increased ductile behavior (white arrow) (*14*). Elevated fluid pressures counteract this thermal effect, ensuring that hydrofracturing always starts from the background value whenever fluid pressure reaches the stress-state–dependent failure criterion (gray dots) (fig. S2) (*10*).

To explore the first-order chemical consequences of this physical process, we defined proxies for copper ore precipitation and quartz vein densities. Experimental data and fluid inclusion studies show that solubilities of copper drop sharply over the pressure and temperature gradients that emerge at the simulated transition zone (*9*, *22*). A copper-enrichment potential for each rock volume was therefore computed by integrating all steps of fluid throughput in which a packet of magmatic fluid cooled through the temperature interval from 450° to 350°C, assuming 100% precipitation, and normalizing this integral to the copper content of the fluid released by a unit volume of source magma (Fig. 4B). Enrichment by a factor of 1000 can be achieved, corresponding to a maximum ore grade of about 2.5 weight percent if a concentration of 500 parts per million extractable copper in the source fluid is assumed (*10*). This proxy provides an upper limit for the natural process, considering that copper extraction at the source may not be complete, and deposition in the ore shell may be somewhat dispersed in a heterogeneously fractured rock mass. The predicted ore shells, coinciding with the areas of sharp gradients in pressure and temperature within the central zone of greatest up-flow, closely resemble the bell-shape of many porphyry ore shells, including their characteristic sharp variations of ore grade near the top and the more gradual decrease down their limbs (Fig. 1A).

A proxy for quartz vein-volume can be calculated by integrating all steps of permeability increase, converting it into a pore space increase by using a cubic law relation (*10*). We did not model chemical precipitation but assumed that this space would be filled by quartz, which makes this proxy an upper limit for actual vein density. The modeled patterns of the vein-volume potential exhibit the characteristic relation to the ore shells as seen in natural systems (Figs. 1 and 4B). High vein density overlaps with predicted copper enrichment near the sharp top and upper flanks of

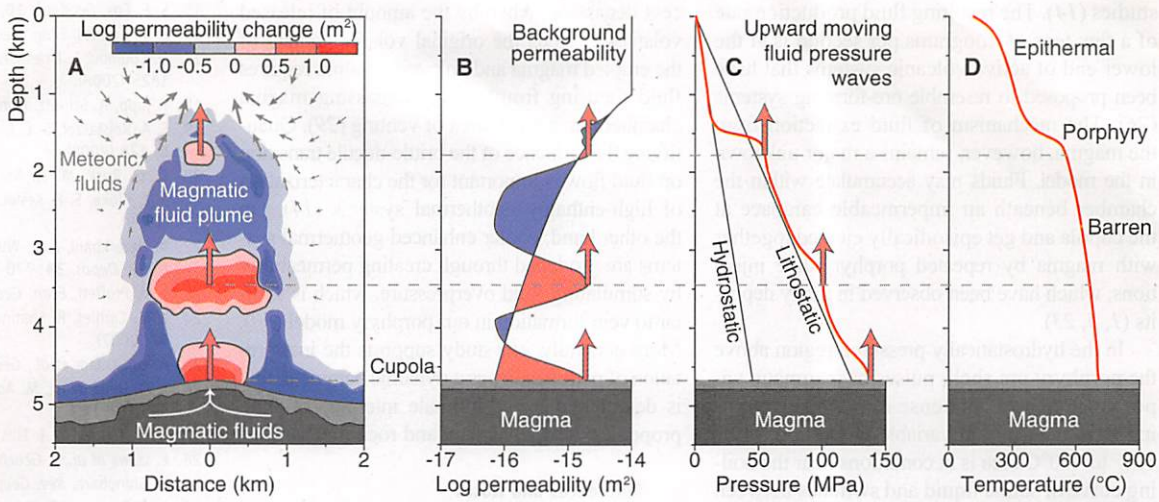

Fig. 3. Model results after 5000 years when a magmatic fluid plume with a stable temperature-pressure front is established. **(A)** Magmatic fluids ascend with permeability-overpressure waves (red), while heat removal by steady convection of meteoric fluids (gray arrows) focuses and stabilizes the plume. Fluid pulses travel through the lithostatically pressured part within a few years; the exact period depends on the parameterization of hydrofracturing and fluid supply rates (*10*). **(B)** Permeability waves reflect the responses of the rock to temperature and fluid pressure (Fig. 2). **(C)** Fluid pressure distribution varies from essentially lithostatic in the inner part to hydrostatic in the uppermost part. **(D)** Temperatures and pressures in the dynamic interior of the magmatic plume are too high for ore mineralization (barren core), until a sharp drop along a near-stationary front creates the environment for porphyry-type ore formation, followed by further cooling to epithermal conditions.

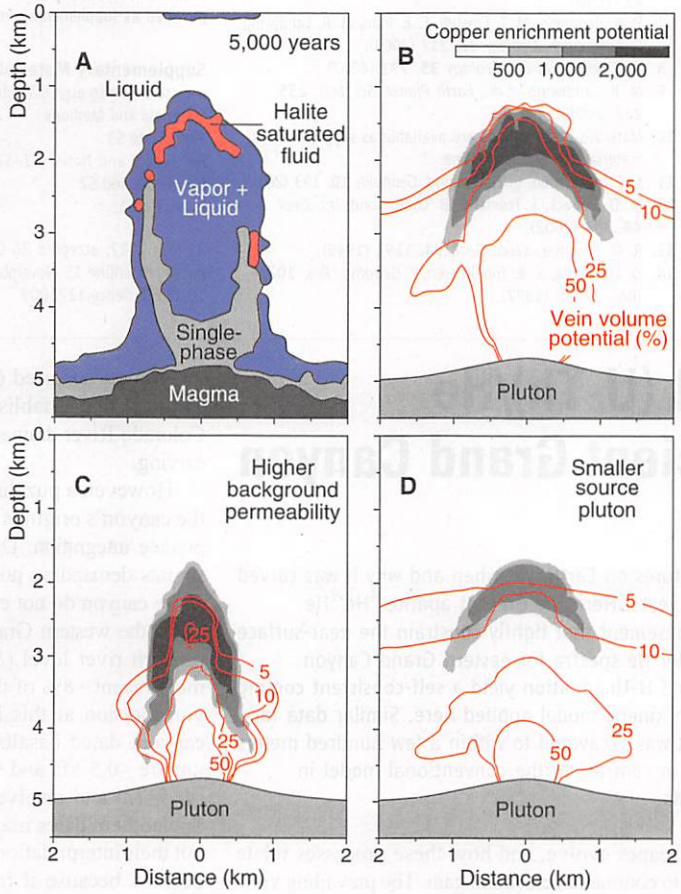

Fig. 4. Fluid phase states and integrated mineralization predicted by the model. **(A)** Hot and lithostatically pressured primary fluids are injected into the host rock as a single-phase ("supercritical") fluid of intermediate density, then phase-separate into highly saline liquid and vapor on ascent and locally saturate solid halite because of the drop in temperature and pressure (Fig. 3). Precipitated halite is modeled as immobile and hence will accumulate and partially block pore space until it is dissolved again, either by surrounding fluids or by temperature or pressure changes (*10*). **(B)** Modeled copper-enrichment potential and vein-volume potential, integrated over the simulation period, serve as proxies for ore shells and vein densities. Models **(C)** and **(D)** illustrate variations in permeability and fluid source rate.

the ore shells but extends and increases to greater depth into the barren core, which is consistent with observations at Bingham Canyon (*6*), Bajo de la Alumbrera (*23*), and many other deposits.

The temporal relations between the quartz and copper proxies also resolve previously unexplained field observations. The bulk of the vein-volume potential is established rapidly during the initial simulation stages, whereas the copper-enrichment potential accumulates more gradually after the magmatic fluid plume has stabilized (movie S2). This prediction describes a physical process for observations showing that copper deposition is texturally later than the main mass of vein quartz (*7*) and with indications that early quartz veining with related potassic alteration acted on shorter time scales (*24*). As the fluid supply slowly decreases with the crystallization of the pluton, the magmatic fluid plume gradually retreats (fig. S3), controlling the vertical extent of the ore shell (Fig. 4B).

To test the sensitivity of the results to geologic factors, we modified the simulation configuration, first by varying permeability (Fig. 4C). Increasing background permeability by one order of magnitude results in a narrower and vertically more extensive enrichment zone. The downward limbs start to merge and may eventually result in a near-cylindrical ore body comparable with the one at Yerington (Fig. 1B). In a second variation, with a source pluton of half the size but identical geometry in our 2D profile (*10*), the resultant copper-enrichment and vein-volume potentials are reduced but show the same patterns and aspect ratios (Fig. 4, B and D).

These variations suggest that the width of the barren core develops independently from the width of the injection zone of the cupola (600 m) and that the host rock permeability has a stronger effect on narrowing this zone than does a reduced fluid supply rate. The width and height of the upflow result from self-organization of the system. The vertical extent of the high-permeability profile is especially remarkable. Higher background permeabilities result in a more effective cooling by more vigorous external convection, and magmatic fluids can be expelled faster, eventually resulting in a stronger focusing effect. This explains why ore bodies are typically centered on porphyry stocks, without showing a correlation between deposit size and the dimension of these small intrusions (*1*).

The time scale of ore formation is between 50,000 and 100,000 years, which is in good agreement with geochronology (*25*) and earlier modeling

studies (*14*). The resulting fluid production rate of a few tens of kilograms per second is at the lower end of active volcanic systems that have been proposed to resemble ore-forming systems (*26*). The mechanism of fluid extraction from the magma, however, remains a major unknown in the model. Fluids may accumulate within the chamber beneath an impermeable carapace at the cupola and get episodically ejected together with magma by repeated porphyry-dike injections, which have been observed in many deposits (*1*, *5*, *23*).

In the hydrostatically pressured region above the porphyry ore shell, pulses of magmatic vapor episodically condense into the surrounding fluids and mix in variable proportions. This 100° to 400°C area is at conditions near the boiling curve of saline liquid and switches between a single-phase liquid state (as in Fig. 4A) and a continuous two-phase zone with locally restricted, vapor-dominated fluid lenses rising to the surface. Predicted temperature and pressure conditions are characteristic for acid alteration that overlaps with the tops of some porphyry deposits (*1*) and provide a physical link to epithermal gold mineralization (Fig. 3D) (*27*). These vein deposits often show evidence for episodic boiling events, and gold precipitation is confined to thin layers (*28*), possibly correlating with minor admixing of magmatic fluid pulses in the simulations.

The self-stabilizing process of focused fluid release from large magma chambers also sheds new light on the hydrological dynamics of active volcanoes and sources of geothermal energy. Excess degassing, whereby the amount of released volatiles exceeds the original volatile content of the erupted magma and volcanic conduit, requires fluid focusing from a large degassing magma chamber into a small area of venting (*29*). Quantifying the influence of the brittle-ductile transition on fluid flow is important for the characterization of high-enthalpy geothermal systems (*14*). On the other hand, cooler enhanced geothermal systems are produced through creating permeability by stimulating fluid overpressure, which is similar to vein formation in our porphyry model (*30*). More generally, our study supports the interpretation of permeability as a dynamic parameter that is determined by an intimate interplay of fluid properties, heat advection, and rock mechanics.

References and Notes

1. R. H. Sillitoe, *Econ. Geol.* **105**, 3 (2010).
2. J. W. Hedenquist, J. B. Lowenstern, *Nature* **370**, 519 (1994).
3. R. W. Henley, A. McNabb, *Econ. Geol.* **73**, 1 (1978).
4. J. Arif, T. Baker, *Miner. Depos.* **39**, 523 (2004).
5. J. H. Dilles, *Econ. Geol.* **82**, 1750 (1987).
6. G. Gruen, C. A. Heinrich, K. Schroeder, *Econ. Geol.* **105**, 69 (2010).
7. P. B. Redmond, M. T. Einaudi, E. E. Inan, M. R. Landtwing, C. A. Heinrich, *Geology* **32**, 217 (2004).
8. R. J. Bodnar *et al.*, *Geology* **35**, 791 (2007).
9. M. R. Landtwing *et al.*, *Earth Planet. Sci. Lett.* **235**, 229 (2005).
10. Materials and methods are available as supplementary materials on *Science* Online.
11. S. E. Ingebritsen, C. E. Manning, *Geofluids* **10**, 193 (2010).
12. M. D. Zoback, J. Townend, B. Grollimund, *Int. Geol. Rev.* **44**, 383 (2002).
13. R. O. Fournier, *Econ. Geol.* **94**, 1193 (1999).
14. D. O. Hayba, S. E. Ingebritsen, *J. Geophys. Res.* **102**, (B6), 12235 (1997).
15. S. F. Cox, *Geofluids* **10**, 217 (2010).
16. L. M. Cathles, *Econ. Geol.* **88**, 1977 (1993).
17. D. Coumou, T. Driesner, C. A. Heinrich, *Science* **321**, 1825 (2008).
18. T. Jupp, A. Schultz, *Nature* **403**, 880 (2000).
19. S. A. Rojstaczer, S. E. Ingebritsen, D. O. Hayba, *Geofluids* **8**, 128 (2008).
20. B. G. Rusk, M. H. Reed, *Geology* **30**, 727 (2002).
21. P. L. Cloke, S. E. Kesler, *Econ. Geol.* **74**, 1823 (1979).
22. A. Hezarkhani, A. E. Williams-Jones, C. H. Gammons, *Miner. Depos.* **34**, 770 (1999).
23. J. M. Proffett, *Econ. Geol.* **98**, 1535 (2003).
24. L. M. Cathles, R. Shannon, *Earth Planet. Sci. Lett.* **262**, 92 (2007).
25. A. von Quadt *et al.*, *Geology* **39**, 731 (2011).
26. J. W. Hedenquist, M. Aoki, H. Shinohara, *Geology* **22**, 585 (1994).
27. R. W. Henley, A. J. Ellis, *Earth Sci. Rev.* **19**, 1 (1983).
28. E. Izawa *et al.*, *J. Geochem. Explor.* **36**, 1 (1990).
29. H. Shinohara, *Rev. Geophys.* **46**, RG4005 (2008).
30. K. F. Evans, A. Genter, J. Sausse, *J. Geophys. Res.* **110**, B04204 (2005).

Acknowledgments: This work was supported by the Swiss National Science Foundation. We thank the reviewers for inspiring thoughts on the manuscript. This study benefited from discussions with D. Coumou, S. Cox, J. Dilles, S. Geiger, S. Matthai, and many others. Selected data and code are provided as supplementary materials.

Supplementary Materials

www.sciencemag.org/cgi/content/full/science.1225009/DC1
Materials and Methods
Figs. S1 to S3
References and Notes (*31*–*52*)
Movies S1 and S2
Database S1

21 May 2012; accepted 26 October 2012
Published online 15 November 2012;
10.1126/science.1225009

Apatite $^4He/^3He$ and (U-Th)/He Evidence for an Ancient Grand Canyon

R. M. Flowers[1]* and K. A. Farley[2]

The Grand Canyon is one of the most dramatic features on Earth, yet when and why it was carved have been controversial topics for more than 150 years. Here, we present apatite $^4He/^3He$ thermochronometry data from the Grand Canyon basement that tightly constrain the near-surface cooling history associated with canyon incision. $^4He/^3He$ spectra for eastern Grand Canyon apatites of differing He date, radiation damage, and U-Th zonation yield a self-consistent cooling history that substantially validates the He diffusion kinetic model applied here. Similar data for the western Grand Canyon provide evidence that it was excavated to within a few hundred meters of modern depths by ~70 million years ago (Ma), in contrast to the conventional model in which the entire canyon was carved since 5 to 6 Ma.

The very existence of the Grand Canyon (Arizona, United States) (Fig. 1) inspires questions about why rivers sometimes carve canyons, how drainage systems and landscapes evolve, and how these processes relate to continental elevation gain. The prevailing view is that canyon carving occurred after 5 to 6 million years ago (Ma), when detritus derived from the upstream reaches of the Colorado River system first appeared in Grand Wash Trough at the river's western exit from the Colorado Plateau (*1*–*3*). Many consider the absence of such diagnostic deposits before 6 Ma as evidence that the Grand Canyon was not yet excavated (*4*, *5*), with most recent debate focused on how river integration occurred (*5*–*7*). This interpretation assumes that establishment of the integrated Colorado River drainage requires coeval canyon carving.

However, a puzzling array of data hints that the canyon's origin is more complex and could predate integration. Direct geochronologic constraints demanding post–6 Ma formation of the entire canyon do not exist. Dated volcanic rocks drape the western Grand Canyon ≤75 m above modern river level (*8*), constraining only the most recent ~8% of the total ~1000 m of canyon incision at this location. For the eastern canyon, dated basalts, travertines, and alluvium are ≤0.5 Ma and <200 m above river level (*4*, *9*–*11*) and resolve <20% of total incision. Speleothem dates may extend this record (*12*), but their interpretation as incision constraints is debated because it relies on unproven paleohydraulic assumptions (*4*, *13*). A western canyon speleothem date 290 m above river level suggests that the lower ~30% of western canyon carving occurred after ~3.9 Ma (*12*). Thus, the upper ~70% of the western Grand Canyon lacks any direct geochronologic constraint on when it was carved. In the eastern part of the canyon, 2.19- to 3.72-Ma speleothems located ~900 m above the river (*12*) imply that the majority of the 1500 m

[1]Department of Geological Sciences, University of Colorado at Boulder, 2200 Colorado Avenue, UCB 399, Boulder, CO 80309, USA. [2]Division of Geological and Planetary Sciences, California Institute of Technology, MS 170-25, Pasadena, CA 91125, USA.

*To whom correspondence should be addressed. E-mail: rebecca.flowers@colorado.edu